Metabolic Profiling of Glioblastoma Stem Cells Reveals Pyruvate Carboxylase as a Critical Survival Factor and Potential Therapeutic Target

Ophélie Renoult, Mélanie Laurent–Blond, Hala Awada, Lisa Oliver, Noémie Joalland, Mikaël Croyal, François Paris, Catherine Gratas, Claire Pecqueur

Metabolic Profiling of Glioblastoma Stem Cells Reveals Pyruvate Carboxylase as a Critical Survival Factor and Potential Therapeutic Target

Ophélie Renoult[1], Mélanie Laurent--Blond[1], Hala Awada[1 3], Lisa Oliver[1 2], Noémie Joalland[1], Mikaël Croyal[5 6], François Paris[1 4], Catherine Gratas[1 2], Claire Pecqueur[1 *]

[1] Nantes Université, Inserm 1307, CNRS 6075, Université d'Angers, CRCI2NA, F-44000 Nantes, France ; [2] Centre Hospitalier Universitaire de Nantes, 44093 Nantes, France ; [3] Faculty of Sciences, Lebanese University, Hadath, Beirut, Lebanon ; [4] Institut de Cancérologie de l'Ouest, 44800 Saint-Herblain, France ; [5] Université de Nantes, CNRS, INSERM, l'institut du thorax, F-44000 Nantes, France. ; [6] Université de Nantes, CHU Nantes, Inserm, CNRS, SFR Santé, Inserm UMS 016, CNRS UMS 3556, F-44000 Nantes, France.

[*]Corresponding author : Claire Pecqueur CRCI2NA, Nantes Université, INSERM U1307, CNRS 6075, 8 quai Moncousu 44007 Nantes, France. **E-mail** : claire.pecqueur@univ-nantes.fr; phone (+33)228080302

Declaration of interests

The authors declare no conflict of interest

Abstract

Background: Glioblastoma (GBM) is a highly aggressive tumor with unmet therapeutic needs, which can be explained by extensive intra-tumoral heterogeneity and plasticity. In this study, we aimed to investigate the specific metabolic features of Glioblastoma stem cells (GSC), a rare tumor subpopulation involved in tumor growth and therapy resistance.

Methods: We conducted comprehensive analyses of primary patient-derived GBM cultures and GSC-enriched cultures of human GBM cell lines using state-of-the-art molecular, metabolic and phenotypic studies.

Results: We showed that GSC-enriched cultures display distinct glycolytic profiles compared with differentiated tumor cells. Further analysis revealed that GSC relies on pyruvate carboxylase activity for survival and self-renewal capacity. Interestingly, inhibition of pyruvate carboxylase led to GSC death, particularly when the glutamine pool was low, and increased differentiation. Finally, while GSC displayed resistance to the chemotherapy drug etoposide, genetic or pharmacological inhibition of pyruvate carboxylase restored etoposide sensitivity in GSC, both *in vitro* and in orthotopic murine models.

Conclusion: Our findings demonstrate the critical role of pyruvate carboxylase in GSC metabolism, survival and escape to etoposide. They also highlight pyruvate carboxylase as a therapeutic target to overcome therapy resistance in GBM.

Keywords: Cancer stem cells, glioblastoma, mitochondrial metabolism, pyruvate carboxylation, metabolic vulnerability

Graphical abstract

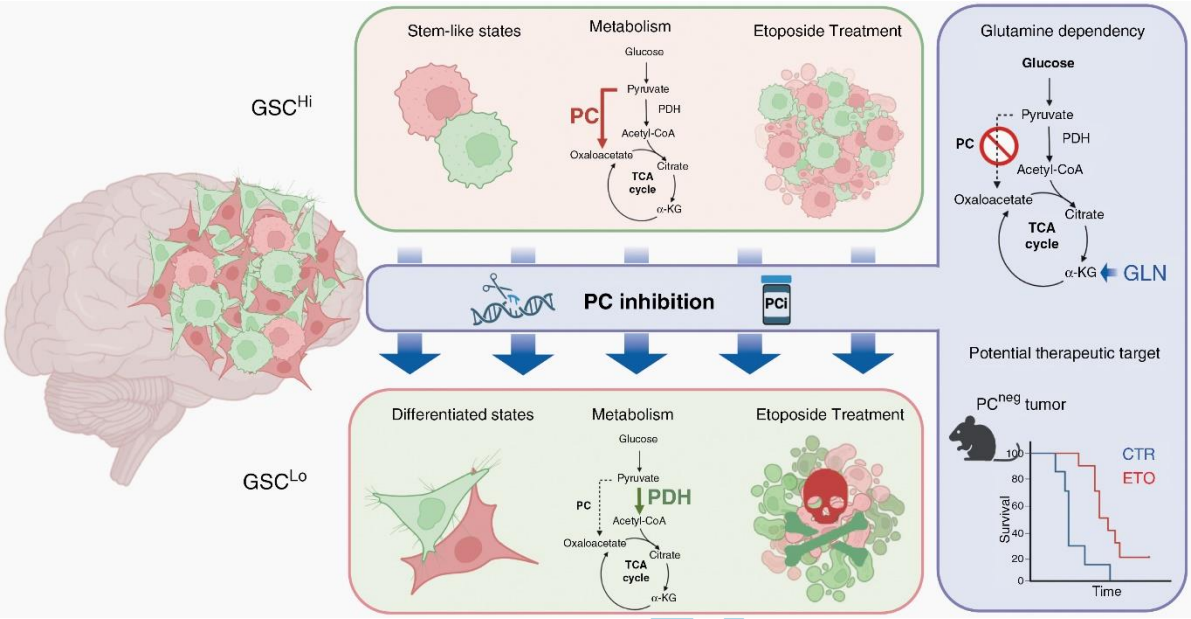

Key bullet points

- Pyruvate carboxylase serves as a metabolic signature to identify GSCs specifically.
- PC inhibition leads to GSC cell death
- Combining etoposide treatment with PC inhibition shows promise as a potential therapeutic strategy to overcome therapy resistance and improve treatment efficacy in GBM.

Importance of the study

Phenotypic and functional heterogeneities are key features of Glioblastoma involved in treatment failure. Glioblastoma stem-like cells (GSC) are considered as the main drivers of tumor heterogeneity, drug resistance, and tumor recurrence. However, the lack of universal GSC markers challenges their identification and eradication. Here, using state-of-the-art molecular, metabolic, and phenotypic studies on primary patient-derived GBM cultures, we revealed that GSCs display distinct metabolic profiles, in particular relying on pyruvate carboxylase-mediated metabolism, which sets them apart from normal cells and bulk tumor cells. Furthermore, its genetic and pharmacological inhibition reduced GSC frequency. Finally, combining etoposide treatment with PC inhibition shows promise as a potential therapeutic strategy to overcome therapy resistance and improve treatment efficacy in GBM.

Introduction

Glioblastoma (GBM) is a highly aggressive primary brain tumor that poses significant challenges in terms of treatment efficacy and patient outcomes. Despite the current standard therapies combining surgery, radiotherapy, and chemotherapy, GBM recurrence remains systematic and patient survival rates are notably poor, with a median survival of 18 months and less than 5% of patients surviving beyond five years [1]. These dismal results can be attributed to various clinical obstacles, including late diagnosis owing to non-specific symptoms, diffuse tumoral infiltration, hidden quiescent states behind the blood-brain barrier, and resistance to conventional therapies.

The intrinsic and dynamic heterogeneity of GBM tumors further complicates the development of effective treatments [2–4]. Molecular heterogeneity within GBM has been characterized through high-throughput transcriptomic profiling conducted by The Cancer Genome Atlas Consortium (TCGA), leading to the identification of three main molecular subtypes: mesenchymal (TCGA-MES), classical (TCGA-CL), and proneural (TCGA-PN) [2,5]. Recent studies have demonstrated that cells of distinct molecular subtypes coexist within the same tumor, defining unique cell states, including neural progenitor-like (NPC), astrocytic-like (AC), mesenchymal-like (MES) states, as well as a cell cycle (CC) signature [6]. Another layer of heterogeneity in GBM arises from the presence of GBM stem cells (GSC) [7,8]. This rare GSC subpopulation contributes to tumor growth, recurrence, and therapy resistance [8,9]. Similar to bulk tumor cells, GSCs may belong to distinct molecular subtypes [10,11]. Therefore, their identification and targeting are critical for developing innovative therapeutic approaches.

GSCs are defined by their ability to self-renew, differentiate into various lineages, and initiate tumor growth, even after serial transplantation. Furthermore, GSCs are highly resistant

to chemotherapy and radiotherapy, in part through increased drug efflux, cell cycle kinetics, enhanced DNA repair, and deregulated differentiation [9,12,13]. However, the identification of these cells remains challenging because current GSC markers, such as CD133, CD15/SSEA1, and A2B5, are not exclusively expressed by GSC [10,12,14–16]. Additionally, GSCs from different molecular subtypes rely on distinct metabolic pathways for growth and survival [17–19]. In particular, some GSCs exhibit enhanced survival abilities in stressful environments such as hypoxic niches with limited oxygen and nutrients [20]. Notably, glucose metabolism plays a crucial role in GSC survival and their metabolic plasticity contributes to therapy resistance [16,21–23]. This inherent metabolic plasticity promotes the enrichment of highly tumorigenic GSC. The limited genetic evolution at recurrence further suggests that resistance mechanisms also largely operate at the phenotypic level [24]. Mirroring molecular tumor cell state transition [6], the dynamic nature of the GSC phenotype allows non-GSC to acquire stem-like characteristics to adapt to microenvironmental conditions [21,25,26]. Understanding GSC metabolism and their reliance on specific metabolic pathways may provide critical insights to develop targeted therapies to overcome therapy resistance in GBM.

In this study, we aimed to investigate the specific metabolic features associated with GSC survival and resistance. We conducted a comprehensive analysis of primary patient-derived GBM cultures (PDC) and GSC-enriched cultures of human GBM cell lines (GSC^{Hi}). Based on their metabolic profiles, we identified significant differences in the glycolytic pathway between GSC^{Hi} and non-GSC tumor cells. In particular, we unveiled the important role of pyruvate carboxylase (PC) in GSC survival, self-renewal, and resistance to chemotherapy. Genetic and pharmacological inhibition of PC induced GSC death and differentiation as well as prevented etoposide resistance, highlighting its potential as a therapeutic target in GBM.

Material and methods

Patient-derived primary cultures (PDC) (Supplementary Table 1) were cultured in Neurobasal media as previously described[17]. All procedures involving human participants were following the ethical standards of the Ethics National Research Committee and with the 1964 Helsinki Declaration and its later amendments or comparable ethical standards. Informed consent was obtained from all individual participants included in this study. Human GBM cell lines were purchased from ATCC and cultured either in complete media [27] or in Neurobasal media. All cell lines are regularly tested for mycoplasma contamination and authenticated using HLA profiling. Gene extinction was realized using the Crispr-Cas9 technology. Cell proliferation and viability were assessed using MTT, Alamar blue, manual cell counting following eosin staining, or using an Incucyte. To evaluate GSC enrichment, sphere formation was investigated by extreme limiting dilution assay (ELDA). Molecular studies were performed by 3' Sequencing RNA Profiling (3'SRP) followed by R package DESeq2 (Bioconductor), Gene Set Enrichment Analysis (GSEA) (deposit on GEO database in progress), and Meta-module analyses (Supplementary Tables 2-4). Protein expression was assessed by immunoblot analysis revelation using a Fusion-FX Spectra imager (Vilber) (Supplementary Table 4). Cell death was investigated using cell viability assay, propidium iodide (PI), or DEVD-GFP probes. Global metabolic studies were performed using XF seahorse Analyzer (Agilent) while metabolomics and fluxomics analyses were performed by LC-HRMS followed by ^{13}C-enrichments using IsoCor software [28]. For *in vivo* experiments, animals were used according to institutional guidelines (Agreement N°17166; Regional Ethics Committee of the Pays de la Loire; France). Tumor cells ($1x10^4$ in 2µL PBS) were orthotopically injected in the subventricular zone of immunodeficient mice as previously described [29]. All results are

presented as mean ± SD from at least four independent experiments. Statistical analyses were performed using Prism 7.0 GraphPad Software. For detailed methods, see the supplementary STAR methods.

Results

Divergent molecular profile and cellular state in patient-derived primary GBM cultures

Patient-derived primary GBM cultures (PDCs) are commonly used to identify potential preclinical targets of GBM. However, while the culture conditions favored GSC maintenance and survival, primary PDCs are highly heterogeneous at the molecular and cellular levels. In this context, we investigated GSC molecular and cellular profiles in PDCs, by analyzing GSC frequency and molecular signature. Using extreme limiting dilution assay (ELDA), we found that all PDCs contained approximately 10-20% of cells capable of self-renewal (**Figure 1A**). RNA sequencing revealed distinct molecular subtypes based on the Cancer Genome Atlas Consortium (TCGA) classification. Six primary PDCs exhibited a mesenchymal subtype (TCGA-MES), four a classical subtype (TCGA-CL), and five a proneural subtype (TCGA-PN) (**Figure 1B**). In agreement with their respective TCGA-subtype, all TCGA-MES cultures exhibited TP53 mutations, whereas EGFR amplification and PTEN loss were more prevalent in the other subtypes (**Supplementary Table 1**). We also assessed the tumor cell state according to the recent meta-modules defined by Neftel et al.[6] (**Supplementary Table 2**). The highest scores for specific tumor cell states corresponded to their respective TCGA subtypes, validating our scoring strategy (**Figure 1B-C**). Indeed, TCGA-MES cultures displayed strong MES scores, whereas TCGA-PN cultures displayed strong NPC scores. Notably, TCGA-MES cultures also displayed strong CC scores. Surprisingly, TCGA-CL cultures exhibited high NPC, MES, and CC scores (**Figure 1C**). Five stemness meta-

modules integrating distinct gene sets were defined based on recent literature to perform stemness scoring [20,30–33](**Supplementary Table 3**) (**Figure 1D-E**). The Venteicher signature displayed the widest score range while the Comba signature showed the narrowest (**Figure 1D**). Notably, the stemness scores of each PDC were highly similar, independently of the meta-module used (**Supplementary Figure 1A**). However, while all PDCs displayed similar GSC frequencies, the stemness scores varied depending on the molecular subtype (**Figure 1E**). The TCGA-PN subtype displayed the lowest stemness score, the TCGA-CL the highest score, and the stemness score showed a linear distribution in the TCGA-MES subtype (**Figure 1E**). Overall, our findings demonstrate great heterogeneity for both the molecular subtypes and cellular states within PDCs, as well as a lack of correlation between the two in our PDC models.

Shared features between GSC from human cell lines and Primary PDC

GSC can be observed in human GBM cell line cells through culture in Neurobasal medium. Accordingly, the GBM cell lines formed neurospheres under these culture conditions (**Figure 1F and Supplementary Figure 1B**). Focusing on U251 cells, we observed that the parental U251 cultures lacked GSC (U251-GSC^{Lo}), while 16.5±2.7% of cells exhibited GSC features when cultured in neurobasal medium (U251-GSC^{Hi}), similar to PDC (**Figure 1G**). Consistent with their stem-like characteristics, U251-GSC^{Hi} re-expressed the stemness marker CD133, while the expression of differentiation markers, such as GFAP and β3-TUB, was lost (**Figure 1H**). Notably, other stemness markers, including Nestin and Sox-2, showed similar expression levels under both culture conditions. Interestingly, U251-GSC^{Hi} also expressed markers associated with GBM aggressiveness and TCGA-MES subtype, including CHI3L1, and CD109 (**Figure 1H**). Importantly, the stemness score of U251-GSC^{Hi} was higher than that of U251-GSC^{Lo} (**Figure 1I**).

To further investigate the relationship between GSC from human cell lines and PDC, we performed 3'SRP RNA sequencing and clustering analysis. Unsupervised hierarchical clustering and principal component analysis (PCA) revealed that U251-GSC^{Hi} clustered with PDC, whereas U251-GSC^{Lo} formed a separate cluster (**Figure 1J**). Notably, the second principal component (PC2) axis defined a continuum of stemness states, ranging from U251-GSC^{Lo} to TCGA-CL/PN PDCs, U251-GSC^{Hi}, and ending with TCGA-MES PDCs (**Figure 1J**). Altogether, our results indicate that U251-GSC^{Hi} share both molecular and functional characteristics with PDCs, suggesting their relevance as a model for studying GSC behavior.

Distinct metabolic profiles between GSC and non-GSC cells.

To explore the metabolic differences between GSC and non-GSC, we conducted global analyses using the Seahorse technology in PDCs, U251-GSC^{Hi}, and U251-GSC^{Lo} (**Figure 2A**). Consistent with their quiescence associated with stem-like characteristics, U251-GSC^{Hi} as well as TCGA-MES and TCGA-CL/PN PDCs exhibited low glycolytic (ECAR) and oxygen consumption (OCR) rates compared to U251-GSC^{Lo}. Accordingly, glucose consumption was significantly higher in U251-GSC^{Lo} than in U251-GSC^{Hi} cultures (**Figure 2B**). Therefore, we investigated the fate of glycolytic pyruvate to understand glucose utilization in GSC and non-GSC cells. The three primary metabolic fates of pyruvate are lactate, alanine, with which pyruvate is in equilibrium, and TCA metabolites that fuel mitochondrial metabolism (**Figure 2C**). Analysis of lactate secretion, intracellular levels of alanine and key TCA metabolites revealed distinct metabolic profiles. U251-GSC^{Lo} exhibited higher lactate secretion, whereas U251-GSC^{Hi} as well as TCGA-MES and TCGA-CL/PN PDCs showed higher intracellular levels of alanine, citrate, and malate (**Figure 2D-F & Supplementary Figure 2**). These findings indicate that U251-GSC^{Lo} primarily relies on

aerobic glycolysis, whereas U251-GSC^{hi} utilizes glycolytic pyruvate to sustain mitochondrial metabolism.

Pyruvate carboxylation is a major metabolic pathway in GSC.

Once in the mitochondria, glycolytic pyruvate is converted to acetyl-CoA by pyruvate dehydrogenase (PDH) (**Figure 3A**). Pyruvate can also be converted to oxaloacetate (OAA) by pyruvate carboxylase (PC), providing an alternative route for glucose utilization. We analyzed citrate isotopologue enrichment using $^{13}C_6$-glucose fluxomics to distinguish between PDH and PC fluxes. Indeed, citrate generated from acetyl-CoA is labeled on two carbons (m+2), whereas the direct carboxylation of pyruvate to OAA by PC generates citrate labeled on three carbons (m+3). Citrate built up from both glycolytic acetyl-CoA (m+2) and glycolytic OAA (m+3) is labeled on five carbons (m+5) (**Figure 3A**). Citrate isotopologue analysis revealed a significant increase in PC-dependent citrate (m+3) in U251-GSC^{Hi} as well as TCGA-MES and TCGA-CL/PN PDCs, in contrast to PC-independent citrate (m+2), which was similar in all cultures (**Figure 3B**). PC activity was then estimated by subtracting succinate (m+3) from malate (m+3) over alanine (m+3) since succinate (m+3) is only generated by an oxidative TCA cycle and alanine is in equilibrium with pyruvate. U251-GSC^{Hi} as well as TCGA-MES and TCGA-CL/PN PDCs exhibited significant PC activity, whereas U251-GSC^{Lo} showed negligible PC activity (**Figure 3C**). However, PC activity varies depending on the molecular subtype. Specifically, TCGA-CL/PN displayed significant but low PC activity, whereas both U251-GSC^{Hi} and TCGA-MES showed high PC activity. In agreement with PC activity, PC expression was strong in U251-GSC^{Hi} and TCGA-MES (**Figure 3D-E**). Its expression was weaker in TCGA-CL/PN, and barely detectable in U251-GSC^{Lo}. In contrast, PDH expression was similar in all cultures. We confirmed the specificity of

PC activity in GSC^{Hi} cultures from various human GBM cell lines. GSC^{Hi} from LN18, U87, and A172 cultures consistently exhibited significantly higher PC activity than GSC^{Lo} ones (**Figure 3F**). To confirm that PC activity was indeed associated with stemness and not due to different culture conditions between GSC^{Hi} and GSC^{Lo}, PC activity was assessed in the presence of different glucose concentrations, various growth factors, and in 2D and 3D culture settings. Our results showed that none of these conditions had a significant effect on PC activity (**Figure 3G**, **Supplementary Figure 3**). These compelling findings strongly support the notion that PC-mediated pyruvate carboxylation is a specific metabolic pathway utilized by GSCs, independently of the experimental settings. Finally, PC activity was measured in relevant normal human cells. PC activity was not detected in three out of four primary astrocyte cultures or in iPS-derived neural stem cells (**Figure 3H**). These results collectively showed the specific association between PC activity and expression with GSC metabolism, emphasizing the significance of PC-mediated pyruvate carboxylation in GSC survival.

PC Inhibition Impairs GSC Survival and Self-Renewal

We used CRISPR-Cas9 technology to knock out the PC gene to evaluate the functional significance of PC in GSC. Both PC expression and activity were completely abolished in U251-GSC^{Hi} following PC knockout (**Figure 4A-B**). Surprisingly, PC knockout led to significant cell death in U251-GSC^{Hi}, as demonstrated by manual cell count (**Supplementary Figure 4A**), PI staining (**Figure 4C**), and caspase activation using the DEVD-GFP probe (**Figure 4D**). In contrast, U251-GSC^{Lo} was not affected by PC knockout (**Figure 4B-C**). Similar results were observed in three different PDCs where PC knockout led to a significant increase in caspases activation (**Figure 4E and Supplementary Figure 4B-F**). We also explored the effects of 3-MCPD, a

pyruvate analogue that cannot be further metabolized by PC. We first confirmed that 3-MCPD inhibited PC activity (**Supplementary Figure 4E**). Treatment with 3-MCPD induced cell death in U251-GSC^{Hi} (**Supplementary Figure 4F-H**) and PDC1 (**Figure 4F**). Finally, in U251-GSC^{Hi}, PC knockout specifically affected the GSC subpopulation, since it reduced the number of cells capable of self-renewal (**Figure 4G**) and increased differentiation markers expression (**Figure 4H**). Altogether, these findings demonstrate the critical role of PC in GSC survival and self-renewal and reinforce the consistent findings across different GSC models.

PC activity releases GSC from glutamine dependency

We investigated whether PC is involved in tumor cell survival under conditions of restrictive nutrient availability, considering that GSCs may be found in hypoxic niches. While hypoxia (1% O2) increased GSC enrichment (**Supplementary Figure 5**A), it also reduced cell proliferation (**Supplementary Figure 5B**). Surprisingly, this effect was independent of PC expression. As PC is involved in glycolytic metabolism, we examined tumor cell survival upon glutamine restriction. While U251-GSC^{Lo} died as glutamine concentration in the medium decreased, U251-GSC^{Hi} survival remained unaffected (**Figure 5A**). Similar experiments were performed following PC knockout to assess PC specific role. PC knockout did not alter U251-GSC^{Lo} proliferation but significantly reduced the ability of U251-GSC^{Hi} to survive under glutamine restriction in a dose-dependent manner (**Figure 5B**). Further investigation into the metabolic changes revealed that PC knockout increased both the glycolytic and oxidative metabolism of U251-GSC^{Hi} specifically (**Figure 5C-D**). Notably, PC knockout promoted mitochondrial anaplerotic metabolism in U251-GSC^{Hi}, as evidenced by increased glutamine fueling of OCR (**Figure 5E-F**) and accumulation of glycolytic alanine (**Figure 5G**). These findings were further supported by the pharmacological

inhibition of PC using 3-MCPD leading to increased cell death upon glutamine deprivation (**Figure 5H**). Similar results were obtained in PDC1 cells knocked out for PC when glutamine was restricted (**Figure 5I**), validating the importance of PC activity in GSC survival under glutamine restriction. Collectively, our results demonstrate that PC plays a pivotal role in releasing GSC from glutamine dependency.

PC inhibition overcomes etoposide resistance in GSC

We have previously reported that sensitivity to etoposide, a chemotherapeutic drug that targets DNA topoisomerase II, relies on mitochondrial anaplerosis. Therefore, we investigated the sensitivity of our GSC models to etoposide. All GSC-enriched cultures, namely U251-GSC^{Hi} and PDC1 cells, exhibited significant resistance to etoposide compared with U251-GSC^{Lo} (IC50: <1 μg/ml for U251-GSC^{Lo}; 21.08±4.3 μg/ml for U251-GSC^{Hi}; >100 μg/ml for PDC1; $p<0.0001$) (**Figure 6A**). Interestingly, in both U251-GSC^{Hi} and U251-GSC^{Lo}, etoposide induced an acute metabolic rewiring, leading to a drastic reduction in mitochondrial respiration and increased glycolysis, as reflected by ECAR (**Supplementary Figure 6A-B**). However, etoposide-induced glycolysis was significantly higher in the GSC models (**Figure 6B**). Interestingly, etoposide treatment also increased PC activity in U251-GSC^{Hi} (**Figure 6C)**. To investigate the effect of PC inhibition on etoposide sensitivity, we performed genetic or pharmacological inhibition of PC in GSC models. Both genetic knockout and pharmacological inhibition of PC restored etoposide sensitivity in U251-GSC^{Hi} (**Figure 6D-F**). The synergy between etoposide and PC inhibition was also observed in PDC1 (**Figure 6G-I**), PDC3 (**Supplementary Figure 6E-F**), and PDC9 (**Supplementary Figure 6G-H**). Notably, etoposide and PC inhibition activated distinct cell death pathways, as demonstrated by PI and DEVD-GFP staining, suggesting that the combination might

be more effective than etoposide alone (**Supplementary Figure 6I**). Finally, this combinatorial strategy was investigated in several murine models of GBM, using either U251-GSC^{Hi}, PDC1, or PDC9. Although etoposide did not affect the survival of mice bearing tumors expressing PC from U251-GSC^{Hi} or PDC1 cultures (**Supplementary Figure 7A-B)**, it significantly increased mouse survival when tumors did not express PC (**Figure 6J**). In contrast, etoposide increased the survival of all mice when tumor cells expressed low or no PC expression, as shown in PDC9-LCV2 and PDC9-PC sg2 experiments (**Supplementary Figure 7A-B**). Our findings demonstrate that inhibiting PC sensitizes GSCs to etoposide and effectively overcomes etoposide resistance. This highlights the promising potential of targeting PC as a therapeutic strategy for treating GBM.

Discussion

GBM prognosis remains dismal because of tumor escape from current treatments. The GSC subpopulation is implicated in GBM recurrence, posing a significant challenge to their identification and targeted elimination. The present study sheds light on the metabolic characteristics of GSCs and their potential role in therapy resistance and tumor recurrence. We demonstrated that GSCs display specific metabolic profiles with a singular reliance on PC-mediated metabolism, which sets them apart from normal cells and bulk tumor cells. We further demonstrated, through genetic and pharmacological inhibition, that PC activity is involved in GSC self-renewal, survival in both rich and nutrient-restrictive environments, and etoposide resistance. Finally, using orthotopic murine models, we revealed that combining etoposide treatment with PC inhibition opens a potential therapeutic strategy to overcome therapy resistance.

The efficient improvement of GBM treatment critically hinges on the effective elimination of GSCs. However, identifying these cells in the clinical setting remains challenging due to their dynamic and reciprocal transitions between differentiated and stem-like states. This results in the presence of both differentiated tumor cells and GSCs, as well as a continuum of cell states between these two states. The lack of universal GSC biomarkers further complicates their identification [34]. While various biomarkers commonly used to identify GSC include CD133, ALDH, CD90, Nestin, and CD44 [12,23], the accuracy of these biomarkers has been a subject of debate, with numerous studies failing to confirm their specificity and reliability [10,14,35]. To tackle this challenge, the development of primary patient-derived cell (PDC) models that promote GSC enrichment has been instrumental, facilitating the discovery of key mechanisms underlying GBM progression [17,20,24,36]. However, inter-patient diversity requires a broad collection of primary PDCs to delineate a representative and robust biological tumor response. Furthermore, understanding the specific mechanisms involved in GSC maintenance and tumor escape becomes even more complex with intrinsic tumor heterogeneity contributing to this diversity. In our study, we addressed this issue by investigating GSCs using both primary PDCs and human GBM cell lines. In line with prior research, our study revealed significant molecular and cellular heterogeneity between and within primary PDCs and human GBM cell lines, with distinct molecular states coexisting within the same culture. We further emphasized the difficulty in identifying *bone-fide* GSC using various molecular signatures. However, we also demonstrated the relevance of GSCs derived from human GBM cell lines as they exhibit shared molecular and phenotypic features with GSCs from primary PDCs. Such models allowed us to pinpoint PC as a critical survival factor involved in GSC self-renewal, survival, and treatment escape. The identification of PC-mediated pyruvate carboxylation in GSCs may provide a novel metabolic signature that might be exploited for their identification.

Metabolic heterogeneity and plasticity are also crucial features involved in GBM recurrence [17,27,37]. Several publications have reported alternative metabolism in GBM cells allowing their survival in drastic environments, such as hypoxic niches. For example, α-KG reductive carboxylation, the reverse reaction of the conventional clockwise step of oxidative decarboxylation exclusively catalyzed through IDH1 and IDH2 enzymes, has been associated with mitochondrial impairment or hypoxia [38–42]. Here, we unveiled the critical role of PC-mediated pyruvate carboxylation in GSC in sustaining mitochondrial metabolism and glucose utilization, even when mitochondria are functional and in a nutrient-rich environment. Through the carboxylation of pyruvate to oxaloacetate, PC provides an alternative metabolism linking energy substrate utilization with tumor progression needs and enabling the metabolic flexibility required for tumor cell resilience to survive and proliferate. Previous studies have reported that PC is crucial to maintaining cell growth and proliferation when tumor cells are defective in mitochondria or under metabolic stress [39,43,44]. However, its relevance in GSC biology remains poorly understood. Our results suggest that this metabolic adaptation is likely a survival mechanism employed by GSCs to cope with harsh microenvironmental conditions. Indeed, in contrast to U251-GSC^{Lo}, which is highly dependent on glutamine for survival, PC activity releases GSC from glutamine dependency. To the best of our knowledge, only a few publications have reported pyruvate carboxylation as a tumor metabolic adaptation [43,45–52]. Most of these publications were limited to non-small cell lung (NSCL) and breast cancers and correlated PC expression with tumor aggressivity or metastasis treatment [43,45–51]. These novel findings contribute to our understanding of the unique GSC metabolic adaptability.

Our study also addressed the issue of therapy resistance in GSC. These cells exhibit unique features that contribute to treatment resistance and tumor recurrence [7,53,54]. The direct implication of mitochondrial metabolism in treatment escape is currently widely accepted. Several successful approaches combining mitochondrial targeting with radiotherapy or chemotherapy have recently been published. For example, resistant cells from acute myeloid leukemia (AML), which are involved in AML recurrence, exhibit very high mitochondrial bioenergetic and oxidative activity [55]. This metabolic adaptation leads to a greater dependency on complex I activity, which can be efficiently targeted in patients. In GBM, genetic or pharmacological knockdown of IDH1 has been reported to slightly sensitize tumor cells to irradiation, the main arm of initial GBM treatment [56]. As with all therapeutic strategies, one of the main challenges of metabolic targeting is to identify specific pathways that are not or barely used by normal cells. In our study, we demonstrated that PC activity is specifically associated with GSC metabolism and barely expressed or used in normal cells [57]. Therefore, it might be exploited as a potential therapeutic target. Interestingly, combining PC inhibition with the chemotherapeutic drug etoposide delayed tumor progression *in vivo*, opening a new strategy for improving treatment efficacy and overcoming therapy resistance in GBM.

In conclusion, our study provides valuable insights into the singular metabolic characteristics of GSC, in particular their reliance on PC-mediated metabolism enabling their metabolic plasticity. Targeting PC may offer a promising therapeutic avenue for eradicating GSC and overcoming therapeutic resistance in GBM. Thus, our study contributes to the growing understanding of GBM biology and opens new possibilities for developing effective treatments to combat this devastating disease.

Funding

This work was supported by Ministère de la Recherche, la Ligue contre le cancer (Comité de Loire Atlantique and Comité de Vendée) and Fondation ARC, the financial support from ITMO cancer of Aviesan within the framework of the 2021-2030 Cancer Control Strategy, on funds administrated by INSERM.

Conflict of interests

The authors declare no conflict of interest

Authors contributions

CP designed research; LO provided primary cultures; OR, MLB, HA, NJ, MC, and CG performed research; OR, CG, and CP analyzed data; OR and CP wrote the manuscript; all authors revised the manuscript.

Data availability

The data will be made available upon reasonable request.

Acknowledgements

This work was supported by Ministère de la Recherche, la Ligue contre le cancer (Comité de Loire Atlantique and Comité de Vendée) and Fondation ARC. We thank the facilities GenoBIRD, Micropicell, Cytocell, Mass Spectrometry of SFR Bonamy, and the biochemistry laboratory of Nantes CHU. With the financial support from ITMO cancer of Aviesan within the framework of

the 2021-2030 Cancer Control Strategy, on funds administrated by INSERM. We thank the LabEX IGO program supported by the National Research Agency (ANR-11-LABX-0016-01) for providing animals. We also thank Laurent David for providing iPS-derived neural stem cells and Malvyne Derkinderen for providing primary human enteric astrocytes.

Ethic approval and consent to participate

Informed consent was obtained from all individual participants included in this study and all procedures were in accordance with the ethical standards of the ethic national research committee and with the 1964 Helsinki declaration and its later amendments or comparable ethical standards. All in vivo experiments were performed according to institutional guidelines (Agreement N°17166; Regional ethics committee of the Pays de la Loire; France).

Data availability statement

All relevant raw data will be freely available to any researcher for non-commercial purposes on request.

References

1. Stupp R, Hegi ME, Mason WP, et al. Effects of radiotherapy with concomitant and adjuvant temozolomide versus radiotherapy alone on survival in glioblastoma in a randomised phase III study: 5-year analysis of the EORTC-NCIC trial. *The Lancet Oncology*. 2009;10(5):459-466. doi:10.1016/S1470-2045(09)70025-7

2. Wang Q, Hu B, Hu X, et al. Tumor Evolution of Glioma-Intrinsic Gene Expression Subtypes Associates with Immunological Changes in the Microenvironment. *Cancer Cell*. 2017;32(1):42-56.e6. doi:10.1016/j.ccell.2017.06.003

3. Patel AP, Tirosh I, Trombetta JJ, et al. Single-cell RNA-seq highlights intratumoral heterogeneity in primary glioblastoma. *Science*. 2014;344(6190):1396-1401. doi:10.1126/science.1254257

4. Meyer M, Reimand J, Lan X, et al. Single cell-derived clonal analysis of human glioblastoma links functional and genomic heterogeneity. *Proc Natl Acad Sci U S A*. 2015;112(3):851-856. doi:10.1073/pnas.1320611111

5. Verhaak RGW, Hoadley KA, Purdom E, et al. Integrated genomic analysis identifies clinically relevant subtypes of glioblastoma characterized by abnormalities in PDGFRA, IDH1, EGFR, and NF1. *Cancer Cell*. 2010;17(1):98-110. doi:10.1016/j.ccr.2009.12.020

6. Neftel C, Laffy J, Filbin MG, et al. An Integrative Model of Cellular States, Plasticity, and Genetics for Glioblastoma. *Cell*. 2019;178(4):835-849.e21. doi:10.1016/j.cell.2019.06.024

7. Lathia JD, Mack SC, Mulkearns-Hubert EE, Valentim CLL, Rich JN. Cancer stem cells in glioblastoma. *Genes Dev*. 2015;29(12):1203-1217. doi:10.1101/gad.261982.115

8. Gimple RC, Bhargava S, Dixit D, Rich JN. Glioblastoma stem cells: lessons from the tumor hierarchy in a lethal cancer. *Genes Dev*. 2019;33(11-12):591-609. doi:10.1101/gad.324301.119

9. Garnier D, Renoult O, Alves-Guerra MC, Paris F, Pecqueur C. Glioblastoma Stem-Like Cells, Metabolic Strategy to Kill a Challenging Target. *Front Oncol*. 2019;9:118. doi:10.3389/fonc.2019.00118

10. Lottaz C, Beier D, Meyer K, et al. Transcriptional profiles of CD133+ and CD133- glioblastoma-derived cancer stem cell lines suggest different cells of origin. *Cancer Res*. 2010;70(5):2030-2040. doi:10.1158/0008-5472.CAN-09-1707

11. Mao P, Joshi K, Li J, et al. Mesenchymal glioma stem cells are maintained by activated glycolytic metabolism involving aldehyde dehydrogenase 1A3. *Proc Natl Acad Sci USA*. 2013;110(21):8644-8649. doi:10.1073/pnas.1221478110

12. Bao S, Wu Q, McLendon RE, et al. Glioma stem cells promote radioresistance by preferential activation of the DNA damage response. *Nature*. 2006;444(7120):756-760. doi:10.1038/nature05236

13. Chen J, Li Y, Yu TS, et al. A restricted cell population propagates glioblastoma growth after chemotherapy. *Nature*. 2012;488(7412):522-526. doi:10.1038/nature11287

14. Wang J, Sakariassen PØ, Tsinkalovsky O, et al. CD133 negative glioma cells form tumors in nude rats and give rise to CD133 positive cells. *Int J Cancer*. 2008;122(4):761-768. doi:10.1002/ijc.23130

15. Dirkse A, Golebiewska A, Buder T, et al. Stem cell-associated heterogeneity in

Glioblastoma results from intrinsic tumor plasticity shaped by the microenvironment. *Nat Commun*. 2019;10(1):1787. doi:10.1038/s41467-019-09853-z

16. Flavahan WA, Wu Q, Hitomi M, et al. Brain tumor initiating cells adapt to restricted nutrition through preferential glucose uptake. *Nat Neurosci*. 2013;16(10):1373-1382. doi:10.1038/nn.3510

17. Oizel K, Chauvin C, Oliver L, et al. Efficient Mitochondrial Glutamine Targeting Prevails Over Glioblastoma Metabolic Plasticity. *Clin Cancer Res*. 2017;23(20):6292-6304. doi:10.1158/1078-0432.CCR-16-3102

18. Hoang- Minh LB, Siebzehnrubl FA, Yang C, et al. Infiltrative and drug- resistant slow-cycling cells support metabolic heterogeneity in glioblastoma. *EMBO J*. 2018;37(23):e98772. doi:10.15252/embj.201798772

19. Kumar S, Visvanathan A, Arivazhagan A, Santhosh V, Somasundaram K, Umapathy S. Assessment of Radiation Resistance and Therapeutic Targeting of Cancer Stem Cells: A Raman Spectroscopic Study of Glioblastoma. *Analytical Chemistry*. Published online September 14, 2018. doi:10.1021/acs.analchem.8b02879

20. Jin X, Kim LJY, Wu Q, et al. Targeting glioma stem cells through combined BMI1 and EZH2 inhibition. *Nature Medicine*. 2017;23(11):1352-1361. doi:10.1038/nm.4415

21. Pelaz SG, Jaraíz-Rodríguez M, Álvarez-Vázquez A, et al. Targeting metabolic plasticity in glioma stem cells in vitro and in vivo through specific inhibition of c-Src by TAT-Cx43266-283. *eBioMedicine*. 2020;62. doi:10.1016/j.ebiom.2020.103134

22. Galli R, Binda E, Orfanelli U, et al. Isolation and Characterization of Tumorigenic, Stem-

like Neural Precursors from Human Glioblastoma. *Cancer Res*. 2004;64(19):7011-7021. doi:10.1158/0008-5472.CAN-04-1364

23. Singh SK, Hawkins C, Clarke ID, et al. Identification of human brain tumour initiating cells. *Nature*. 2004;432(7015):396-401. doi:10.1038/nature03128

24. Lee J, Kotliarova S, Kotliarov Y, et al. Tumor stem cells derived from glioblastomas cultured in bFGF and EGF more closely mirror the phenotype and genotype of primary tumors than do serum-cultured cell lines. *Cancer Cell*. 2006;9(5):391-403. doi:10.1016/j.ccr.2006.03.030

25. Carnero A, Lleonart M. The hypoxic microenvironment: A determinant of cancer stem cell evolution. *Bioessays*. 2016;38 Suppl 1:S65-74. doi:10.1002/bies.201670911

26. Silva MID, Stringer BW, Bardy C. Neuronal and tumourigenic boundaries of glioblastoma plasticity. *Trends in Cancer*. 2022;0(0). doi:10.1016/j.trecan.2022.10.010

27. Oizel K, Gratas C, Nadaradjane A, Oliver L, Vallette FM, Pecqueur C. D-2-Hydroxyglutarate does not mimic all the IDH mutation effects, in particular the reduced etoposide-triggered apoptosis mediated by an alteration in mitochondrial NADH. *Cell Death Dis*. 2015;6:e1704. doi:10.1038/cddis.2015.13

28. Millard P, Delépine B, Guionnet M, Heuillet M, Bellvert F, Létisse F. IsoCor: isotope correction for high-resolution MS labeling experiments. *Bioinformatics*. 2019;35(21):4484-4487. doi:10.1093/bioinformatics/btz209

29. Chauvin C, Joalland N, Perroteau J, et al. NKG2D Controls Natural Reactivity of Vγ9Vδ2 T Lymphocytes against Mesenchymal Glioblastoma Cells. *Clin Cancer Res*.

2019;25(23):7218-7228. doi:10.1158/1078-0432.CCR-19-0375

30. Venteicher AS, Tirosh I, Hebert C, et al. Decoupling genetics, lineages, and microenvironment in IDH-mutant gliomas by single-cell RNA-seq. *Science*. 2017;355(6332):eaai8478. doi:10.1126/science.aai8478

31. Jiang L, Hao Y, Shao C, et al. ADAR1-mediated RNA editing links ganglioside catabolism to glioblastoma stem cell maintenance. *J Clin Invest*. 2022;132(6):e143397. doi:10.1172/JCI143397

32. Comba A, Faisal SM, Dunn PJ, et al. Spatiotemporal analysis of glioma heterogeneity reveals COL1A1 as an actionable target to disrupt tumor progression. *Nat Commun*. 2022;13(1):3606. doi:10.1038/s41467-022-31340-1

33. Castellan M, Guarnieri A, Fujimura A, et al. Single-cell analyses reveal YAP/TAZ as regulators of stemness and cell plasticity in Glioblastoma. *Nat Cancer*. 2021;2(2):174-188. doi:10.1038/s43018-020-00150-z

34. Prager BC, Bhargava S, Mahadev V, Hubert CG, Rich JN. Glioblastoma Stem Cells: Driving Resilience through Chaos. *Trends Cancer*. 2020;6(3):223-235. doi:10.1016/j.trecan.2020.01.009

35. Chen R, Nishimura MC, Bumbaca SM, et al. A hierarchy of self-renewing tumor-initiating cell types in glioblastoma. *Cancer Cell*. 2010;17(4):362-375. doi:10.1016/j.ccr.2009.12.049

36. Tardito S, Oudin A, Ahmed SU, et al. Glutamine synthetase activity fuels nucleotide biosynthesis and supports growth of glutamine-restricted glioblastoma. *Nat Cell Biol*.

2015;17(12):1556-1568. doi:10.1038/ncb3272

37. Oizel K, Yang C, Renoult O, et al. Glutamine uptake and utilization of human mesenchymal glioblastoma in orthotopic mouse model. *Cancer Metab*. 2020;8:9. doi:10.1186/s40170-020-00215-8

38. Metallo CM, Gameiro PA, Bell EL, et al. Reductive glutamine metabolism by IDH1 mediates lipogenesis under hypoxia. *Nature*. Published online November 20, 2011. doi:10.1038/nature10602

39. Mullen AR, Wheaton WW, Jin ES, et al. Reductive carboxylation supports growth in tumour cells with defective mitochondria. *Nature*. 2012;481(7381):385-388. doi:10.1038/nature10642

40. Gaude E, Schmidt C, Gammage PA, et al. NADH Shuttling Couples Cytosolic Reductive Carboxylation of Glutamine with Glycolysis in Cells with Mitochondrial Dysfunction. *Molecular Cell*. 2018;69(4):581-593.e7. doi:10.1016/j.molcel.2018.01.034

41. Alzial G, Renoult O, Paris F, Gratas C, Clavreul A, Pecqueur C. Wild-type isocitrate dehydrogenase under the spotlight in glioblastoma. *Oncogene*. 2022;41(5):613-621. doi:10.1038/s41388-021-02056-1

42. Wise DR, Ward PS, Shay JES, et al. Hypoxia promotes isocitrate dehydrogenase-dependent carboxylation of α-ketoglutarate to citrate to support cell growth and viability. *Proc Natl Acad Sci USA*. 2011;108(49):19611-19616. doi:10.1073/pnas.1117773108

43. Cheng T, Sudderth J, Yang C, et al. Pyruvate carboxylase is required for glutamine-independent growth of tumor cells. *Proceedings of the National Academy of Sciences of the*

United States of America. 2011;108(21):8674-8679. doi:10.1073/pnas.1016627108

44. Wang J, Sun X, Wang J, et al. NDRG2 inhibits pyruvate carboxylase-mediated anaplerosis and combines with glutamine blockade to inhibit the proliferation of glioma cells. *Am J Cancer Res*. 2022;12(8):3729-3744.

45. Lin Q, He Y, Wang X, et al. Targeting Pyruvate Carboxylase by a Small Molecule Suppresses Breast Cancer Progression. *Advanced Science*. 2020;7(9). doi:10.1002/advs.201903483

46. Sellers K, Fox MP, Bousamra M, et al. Pyruvate carboxylase is critical for non–small-cell lung cancer proliferation. *J Clin Invest*. 2015;125(2):687-698. doi:10.1172/JCI72873

47. Lao-On U, Rojvirat P, Chansongkrow P, et al. c-Myc directly targets an over-expression of pyruvate carboxylase in highly invasive breast cancer. *Biochimica et Biophysica Acta (BBA) - Molecular Basis of Disease*. 2020;1866(3):165656. doi:10.1016/j.bbadis.2019.165656

48. Ma MZ, Zhang Y, Weng MZ, et al. Long Noncoding RNA GCASPC, a Target of miR-17-3p, Negatively Regulates Pyruvate Carboxylase-Dependent Cell Proliferation in Gallbladder Cancer. *Cancer Res*. 2016;76(18):5361-5371. doi:10.1158/0008-5472.CAN-15-3047

49. Davidson SM, Papagiannakopoulos T, Olenchock BA, et al. Environment Impacts the Metabolic Dependencies of Ras-Driven Non-Small Cell Lung Cancer. *Cell Metabolism*. 2016;23(3):517-528. doi:10.1016/j.cmet.2016.01.007

50. Phannasil P, Thuwajit C, Warnnissorn M, Wallace JC, MacDonald MJ, Jitrapakdee S. Pyruvate Carboxylase Is Up-Regulated in Breast Cancer and Essential to Support Growth and Invasion of MDA-MB-231 Cells. *PLoS One*. 2015;10(6):e0129848.

doi:10.1371/journal.pone.0129848

51. Fan TWM, Lane AN, Higashi RM, et al. Altered regulation of metabolic pathways in human lung cancer discerned by (13)C stable isotope-resolved metabolomics (SIRM). *Mol Cancer*. 2009;8:41. doi:10.1186/1476-4598-8-41

52. Gondáš E, Kráľová Trančíková A, Dibdiaková K, et al. Immunodetection of Pyruvate Carboxylase Expression in Human Astrocytomas, Glioblastomas, Oligodendrogliomas, and Meningiomas. *Neurochem Res*. 2023;48(6):1728-1736. doi:10.1007/s11064-023-03856-5

53. Rich JN. Cancer Stem Cells in Radiation Resistance. *Cancer Res*. 2007;67(19):8980-8984. doi:10.1158/0008-5472.CAN-07-0895

54. Dagogo-Jack I, Shaw AT. Tumour heterogeneity and resistance to cancer therapies. *Nat Rev Clin Oncol*. 2018;15(2):81-94. doi:10.1038/nrclinonc.2017.166

55. Bosc C, Saland E, Bousard A, et al. Mitochondrial inhibitors circumvent adaptive resistance to venetoclax and cytarabine combination therapy in acute myeloid leukemia. *Nat Cancer*. 2021;2(11):1204-1223. doi:10.1038/s43018-021-00264-y

56. Wahl DR, Dresser J, Wilder-Romans K, et al. Glioblastoma Therapy Can be Augmented by Targeting IDH1-mediated NADPH Biosynthesis. *Cancer Res*. 2017;77(4):960-970. doi:10.1158/0008-5472.CAN-16-2008

57. Cappel DA, Deja S, Duarte JAG, et al. Pyruvate-Carboxylase-Mediated Anaplerosis Promotes Antioxidant Capacity by Sustaining TCA Cycle and Redox Metabolism in Liver. *Cell Metab*. 2019;29(6):1291-1305.e8. doi:10.1016/j.cmet.2019.03.014

58. Qiu Z, Zhao L, Shen JZ, et al. Transcription Elongation Machinery Is a Druggable

Dependency and Potentiates Immunotherapy in Glioblastoma Stem Cells. *Cancer Discov*. 2022;12(2):502-521. doi:10.1158/2159-8290.CD-20-1848

Figure legends

Figure 1: Molecular profile and cellular state in primary patient-derived cultures

A. Stem cell enrichment measured by ELDA in primary PDC. **B.** Molecular characterization of primary PDC. TCGA molecular subtype according to Verhaak and cell states according to Neftel are indicated. **C.** Multiple variable analysis of cell state scores based on NPC, MES and CC genes meta-modules. **D.** Primary PDC score distribution depending on the stemness meta-modules. **E.** Multiple variable analysis of stemness scores in primary PDC depending on the TCGA-molecular subtype, based on stemness gene meta-modules defined by Vencheiter, Qiu and Jiang. **F**. Representative picture of parental U251 cells and U251-GSC^{Hi} cultured in neurobasal medium. **G**. Stem cell enrichment measured by ELDA in U251-GSC^{Lo}, U251-GSC^{Hi}, and primary PDC. Primary PDC are grouped based on their molecular subtype (TCGA-MES vs TCGA-CL/PN). Each dot represents one primary PDC. One-way ANOVA ($n \geq 3$). **H**. Representative immunoblots of markers of stemness, differentiation, and aggressiveness in U251-GSC^{Lo} and U251-GSC^{Hi}. Two independent replicates are shown per condition. **I.** Multiple variable analysis of stemness scores in U251-GSC^{Lo} and U251-GSC^{Hi} based on stemness gene meta-modules defined by Vencheiter et al[30], Qiu et al[58] and Jiang et al.[31]. **E.** PCA plot of U251-GSC^{Lo}, U251-GSC^{Hi}, and primary PDC, using the top 5000 differential genes.

Figure 2: Metabolic profiling of U251-GSC^{Hi}.

A. Glycolytic and oxidative profiles of U251-GSC^{Lo}, U251-GSC^{Hi} and primary PDC using the Seahorse technology. Two primary PDC per molecular subtype are presented. The results are presented as the Oxygen Consumption Rate (OCR) as a function of Extracellular Acidification Rate (ECAR) (n=4). **B.** Glucose consumption of U251-GSC^{Lo}, U251-GSC^{Hi}, cells and primary

PDC over 48 hours. One-way ANOVA (n=3). **C**. Schematic of glycolytic pyruvate fate. **D.** Lactate secretion of U251-GSC^{Lo}, U251-GSC^{Hi}, and primary PDC after 48 hours. Student t-test (n=3). **E-F**. Intracellular abundance of alanine (E) and citrate (F) measured by mass spectrometry over 5 hours. Student t-test (n=3).

Figure 3: Pyruvate carboxylation as a major metabolic pathway in GSC.

A. Schematic representation of mitochondrial pyruvate-derived metabolite fate using $^{13}C_6$-labeled glucose. Glycolytic pyruvate (m+3) can either be converted to acetyl-CoA (m+2) through PDH or converted to OAA (m+3) by pyruvate carboxylase (PC), subsequently resulting in (m+2) or (m+3) TCA intermediates, respectively. **B**. Enrichment of citrate isotopologues from $^{13}C_6$-glucose metabolites in U251-GSC^{Lo}, U251-GSC^{Hi}, and primary PDC. PC-independent (left) and -dependent (right) isotopologues are indicated. Multiple comparison of 2-way ANOVA was performed. p-values are significant only for citrate (m+3) for all GSC^{Hi} cultures when compared to U251-GSC^{Lo} (n=5). **C**. PC activity in U251-GSC^{Lo}, -GSC^{Hi} and primary PDC. One-way ANOVA (n≥5). **D-E.** Representative immunoblots of Pyruvate Dehydrogenase (PDH) and Pyruvate Carboxylase (PC) in U251-GSC^{Lo}, U251-GSC^{Hi} (D) and PDC (E). Two independent replicates are shown per condition for U251 cells, and each lane corresponds to one specific culture for PDC. **F.** PC activity in GSC^{Lo} and GSC^{Hi} cultures of LN18, U87, and A172 human GBM cell lines. Multiple unpaired t-test (n=3). **G.** PC activity of U251-GSC^{Hi} in various concentrations of glucose. One-way ANOVA (n=3). **H.** PC activity in primary human astrocytes and iPS-derived neural stem cells (NSC).

Figure 4: PC inhibition impairs GSC survival and self-renewal.

A. Representative immunoblots of PC following its silencing using the Crispr-CAS9 technology in U251-GSC^{Hi}. Two strand guides, sg1 and sg2, were used to silence PC expression. **B**. PC activity in U251-GSC^{Hi} (red) and U251-GSC^{Lo} (black) depending on PC expression. Paired t-test (n=4). **C**. Cell death was measured by flow cytometry following propidium iodide (PI) staining in U251-GSC^{Hi} (red) and U251-GSC^{Lo} (black) knockout for PC. Two-way ANOVA (n=3). **D-E**. Cell death in U251-GSC^{Hi} (D) and PDC1(E) grown in 3D by fluorescence monitoring with the Incucyte technology using the DEDV-GFP probe to monitor caspases activation. Representative images are presented on the top panel and GFP intensity on the bottom one. Two-Way ANOVA (n=3). $p<0.05$. **F.** Cell death in PDC1-RFP cells grown in 3D following pharmacological PC inhibition by RFP monitoring with the Incucyte technology. Representative images are presented on the top panel while RFP intensity is presented on the bottom one. Two-Way ANOVA (n=3). $P<0.001$ (F). **G.** Stem cell enrichment measured by ELDA in U251-GSC^{Hi} depending on PC expression. One-way ANOVA ($n \geq 3$). **H.** Expression of the differentiation markers GFAP, β3-TUB, and ASCL1 in U251-GSC^{Hi} depending on PC expression. Representative immunoblots are shown (n=3).

Figure 5: PC inhibition impairs GSC survival under glutamine restriction.

A. Cell viability of U251-GSC^{Hi} and U251-GSC^{Lo} in presence of decreasing glutamine concentrations (48h). Two-way ANOVA (n=4 in duplicate). **B**. Cell viability of U251-GSC^{Hi} (red) and U251-GSC^{Lo} (black) with decreasing glutamine concentrations following PC knockout (48h). Two-way ANOVA (n=4). **C**. Aerobic glycolysis in U251-GSC^{Hi} (red) and U251-GSC^{Lo} (black) following PC silencing, as measured by the Seahorse technology. One-way ANOVA ($n \geq 5$ in

duplicate). **D**. Mitochondrial respiration in U251-GSC^{Hi} (red) and U251-GSC^{Lo} (black) following PC silencing, as measured using the Seahorse technology. One-way ANOVA (n≥5 in duplicate). **E**. Relative oxygen consumption rate (OCR) in U251-GSC^{Hi} with time, in absence of glutamine and after glutamine (Gln) injection. **F**. Glutamine-driven OCR in U251-GSC^{Hi} knockout for PC. One-way ANOVA (n=4 in duplicate). **G**. Intracellular abundance of alanine measured by mass spectrometry over 5 hours. One-way ANOVA (n=4 in duplicate). **H**. Viability of U251-GSC^{Hi} following 3-MCPD treatment in presence or absence of glutamine (48h). Two-way ANOVA (n=4). **I**. Viability of primary PDC1 culture following PC knockout in the presence of decreasing concentrations of glutamine (48h). Two-way ANOVA (n=4).

Figure 6: PC inhibition impairs GSC survival after etoposide treatment.

A. Cell viability of U251-GSC^{Lo}, U251-GSC^{Hi}, and primary PDC1 culture with increasing doses of etoposide (48h). Two-way ANOVA (n=3 in quadruplicate). $p<0.01$ for U251-GSC^{Hi} vs. U251-GSC^{Lo}, $p<0.001$ for PDC1 vs. U251-GSC^{Lo}. **B.** Relative aerobic glycolysis (ECAR) in U251-GSC^{Lo}, U251-GSC^{Hi}, and PDC1, PDC3 and PDC9 culture after etoposide injection measured by Seahorse technology. Sidak multiple comparisons (n=10). **C.** PC activity in U251-GSC^{Hi} after etoposide treatment (50 µg/mL, 5h). Paired t-test (n=3 in duplicate). **D**. Cell death was measured by flow cytometry following propidium iodide (PI) staining in U251-GSC^{Hi} following PC silencing. Two-way ANOVA (n=6). **E.** Cell death in 3D- U251-GSC^{Hi} following PC silencing and etoposide, by fluorescence monitoring with the Incucyte technology using the DEDV-GFP probe. Representative images are presented on the left panel while GFP intensity is presented on the right one. Two-Way ANOVA (n=3). $p<0.01$. **F**. Cell viability of U251-GSC^{Hi} following PC inhibition with 3-MCPD (10mM) with increasing doses of etoposide (48h). Two-way ANOVA (n=3 in

duplicate). $p<0.01$. **G-H**. Cell death in PDC1 following PC silencing and etoposide, by cytometry using the PI probe (G) and by fluorescence using the DEDV-GFP probe (H). For fluorescence analysis, representative images are presented on the left panel while GFP intensity is presented on the right panel. Two-Way ANOVA (n=3). $p<0.005$. **I.** Cell viability of PDC1 following PC inhibition with 3-MCPD (10mM) with increasing doses of etoposide (48h). Two-way ANOVA (n=3 in duplicate). $p<0.01$. **J.** Combined effects of PC silencing and etoposide treatment in orthotopic murine models. U251-GSC^{Hi} (middle) or primary PDC1 cultures (right) were injected into mice brains. Vehicule (PBS) or etoposide was injected 1hour later with the same coordinates. Results are presented as survival curve. $n\geq6$ mice/group, log-rank test.

Figure 1

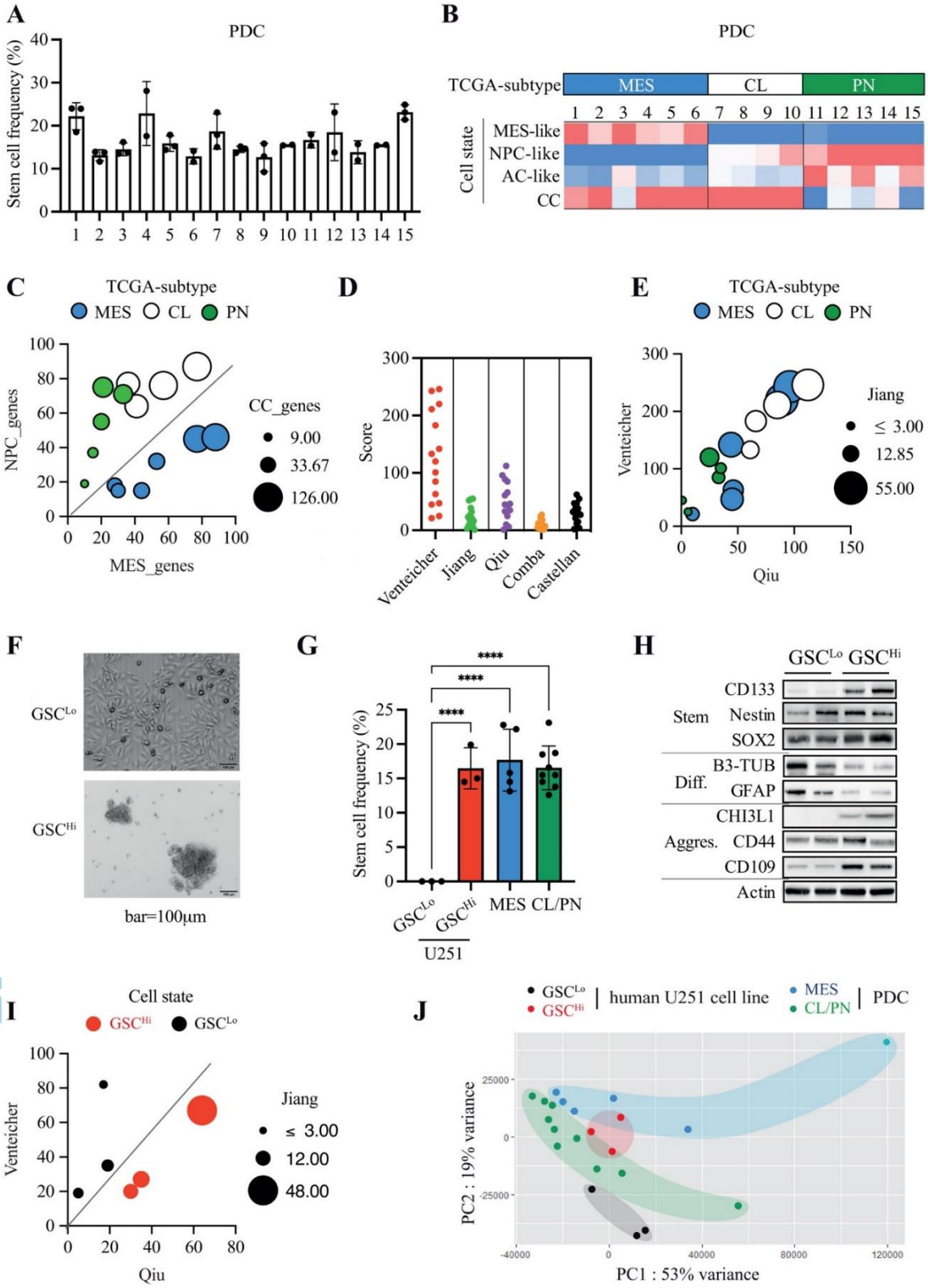

Figure 2

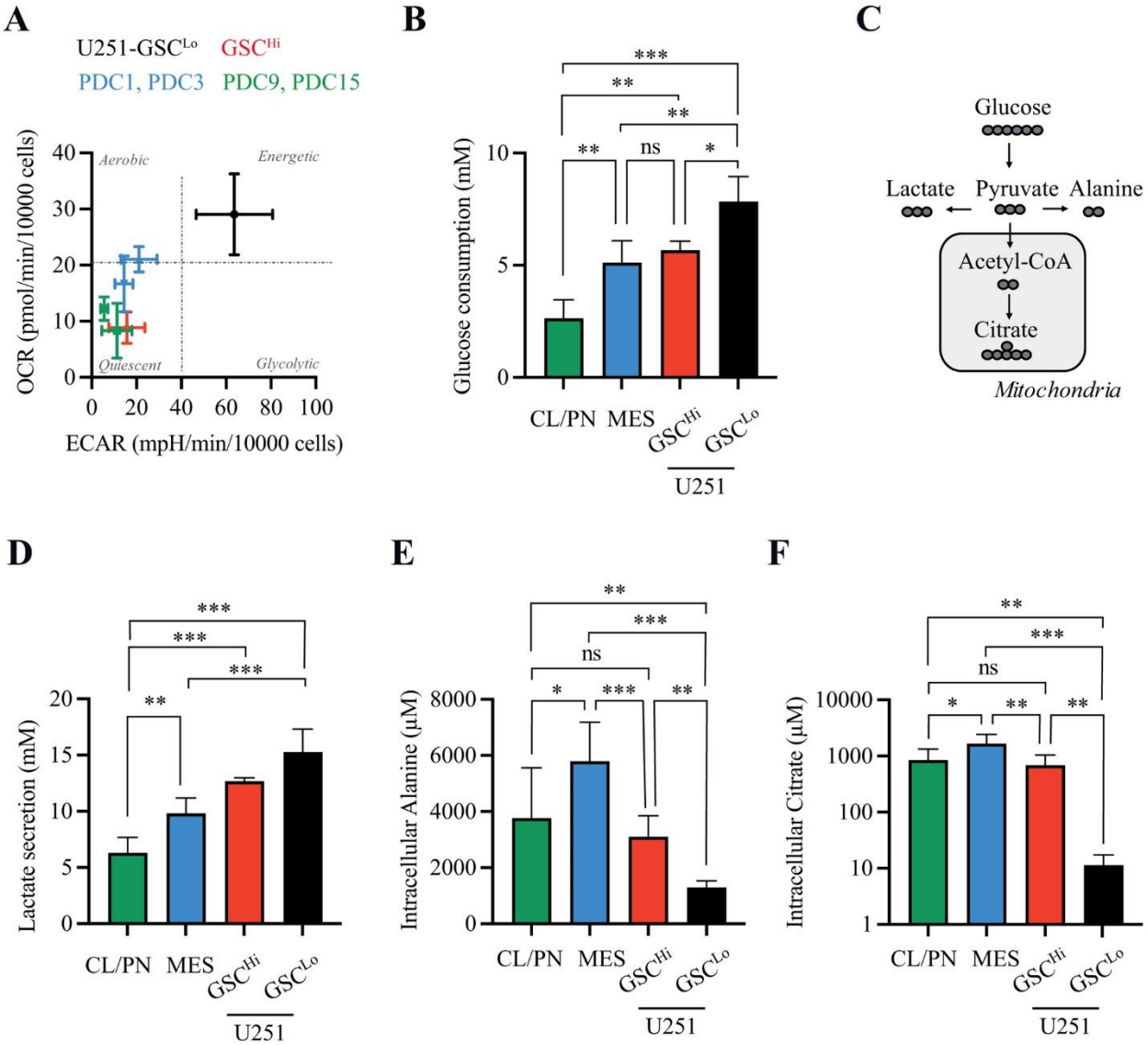

Figure 3

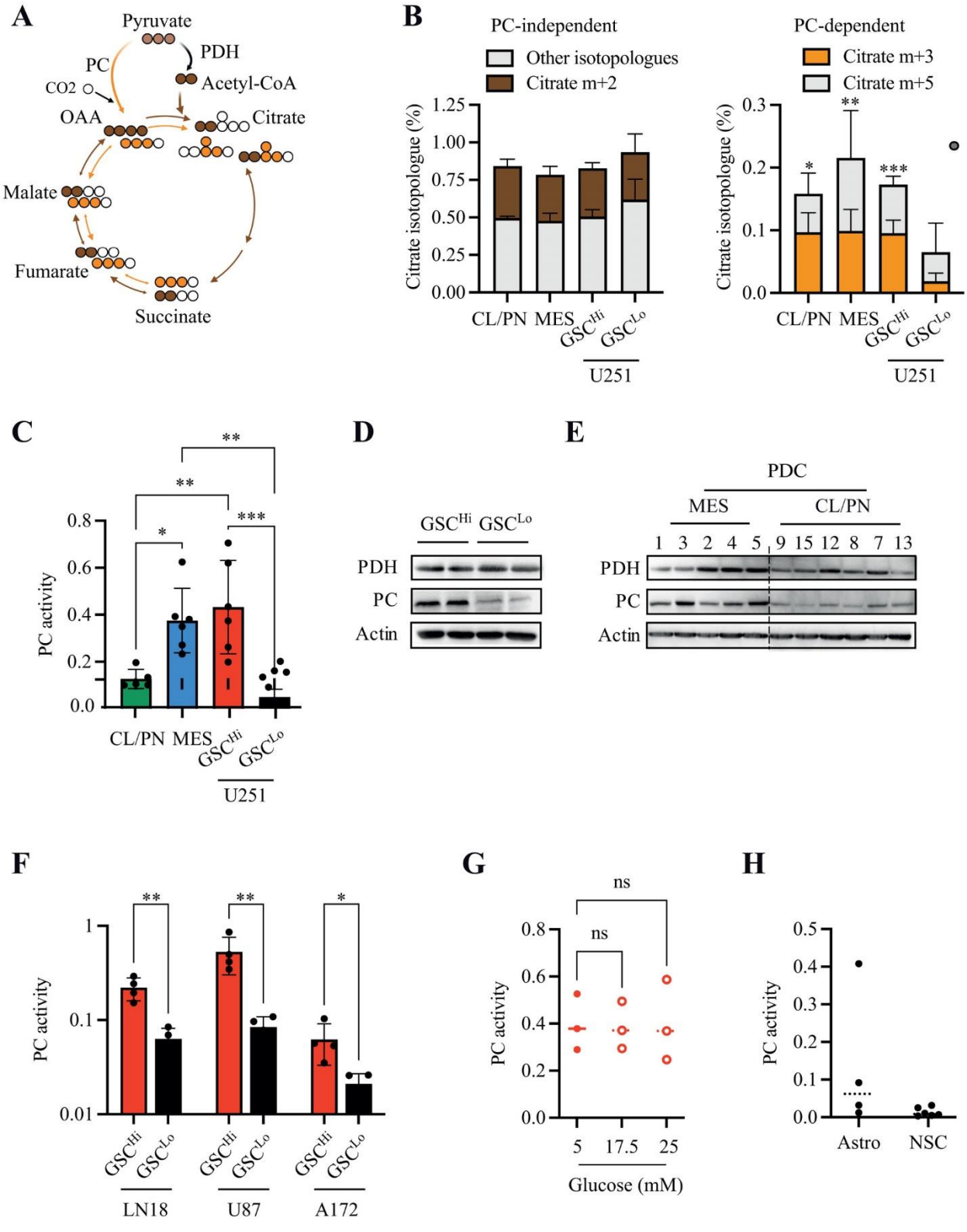

Figure 4

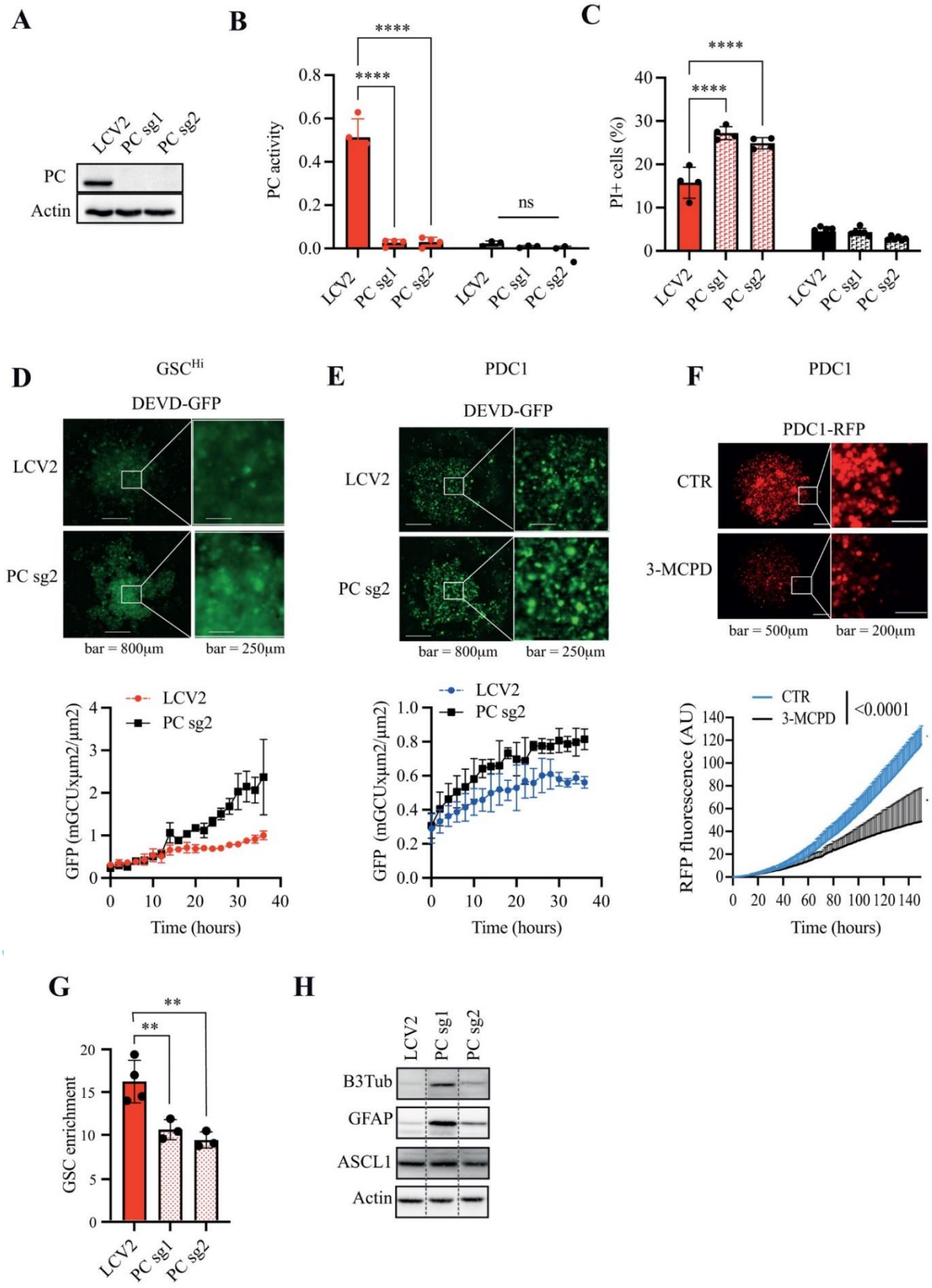

Figure 5

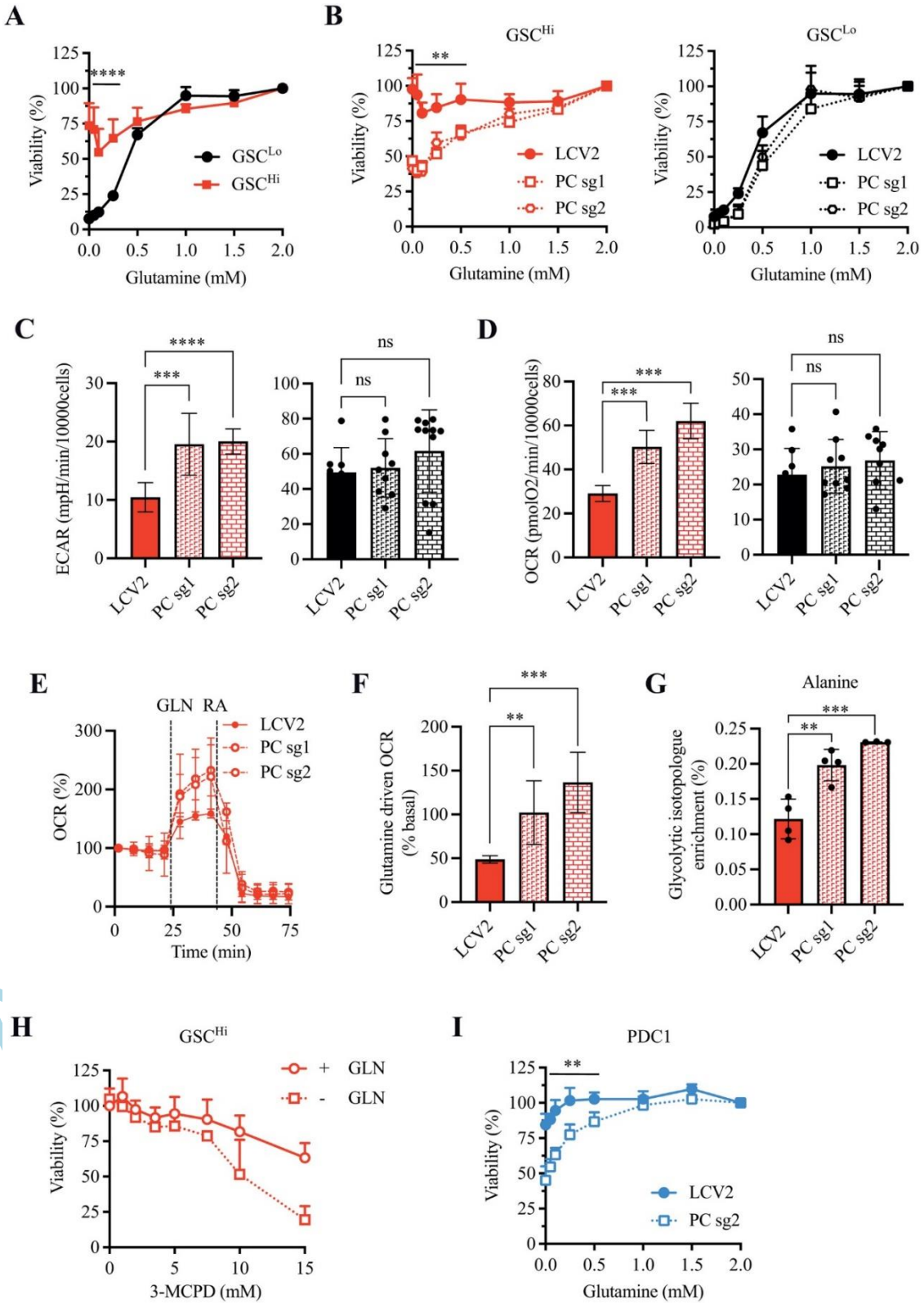

Figure 6